UCSF
UC San Francisco Previously Published Works

Title

Zika Virus Dependence on Host Hsp70 Provides a Protective Strategy against Infection and Disease

Permalink

https://escholarship.org/uc/item/27f1s9vs

Journal

Cell Reports, 26(4)

ISSN

2639-1856

Authors

Taguwa, Shuhei
Yeh, Ming-Te
Rainbolt, T Kelly
et al.

Publication Date

2019

DOI

10.1016/j.celrep.2018.12.095

Peer reviewed

Zika Virus Dependence on Host Hsp70 Provides a Protective Strategy against Infection and Disease

Shuhei Taguwa[1], **Ming-Te Yeh**[2], **T. Kelly Rainbolt**[1], **Arabinda Nayak**[2], **Hao Shao**[3], **Jason E. Gestwicki**[3], **Raul Andino**[2], **Judith Frydman**[1,4,*]

[1]Department of Biology and Genetics, Stanford University, Stanford, CA 94305, USA

[2]Department of Microbiology and Immunology, University of California, San Francisco, San Francisco, CA 94158, USA

[3]Department of Pharmaceutical Chemistry, University of California, San Francisco, San Francisco, CA 94158, USA

[4]Lead Contact

SUMMARY

The spread of mosquito-borne Zika virus (ZIKV), which causes neurological disorders and micro-cephaly, highlights the need for countermeasures against sudden viral epidemics. Here, we tested the concept that drugs targeting host proteostasis pro-vide effective antivirals. We show that different cyto-solic Hsp70 isoforms are recruited to ZIKV-induced compartments and are required for virus replication at pre- and post-entry steps. Drugs targeting Hsp70 significantly reduce replication of different ZIKV strains in human and mosquito cells, including hu-man neural stem cells and a placental trophoblast cell line, at doses without appreciable toxicity to the host cell. By targeting several ZIKV functions, including entry, establishment of active replication complexes, and capsid assembly, Hsp70 inhibitors are refractory to the emergence of drug-resistant virus. Importantly, these drugs protected mouse models from ZIKV infection, reducing viremia, mor-tality, and disease symptoms. Hsp70 inhibitors are thus attractive candidates for ZIKV therapeutics with the added benefit of a broad spectrum of action.

Graphical Abstract

In Brief

Hsp70 inhibitors effectively block Zika virus replication in both human and mosquito cells, without the emergence of drug resistance, and protect mice from lethal ZIKV infection, demonstrating their potential for treatment and prevention of ZIKV disease.

INTRODUCTION

Mosquito-borne viruses pose a major threat to public health. Zika virus (ZIKV), a mosquito-borne flavivirus, spread rapidly throughout the Americas, reaching Puerto Rico and the conti-nental United States (Enfissi et al., 2016; Malone et al., 2016; Weaver et al., 2016). In most cases, ZIKV causes a dengue-like illness, with rashes, conjunctivitis, and other mild clinical mani-festations. ZIKV can also lead to more severe symptoms, including Guillain-Barré syndrome, characterized by progressive weakness, motor dysfunction, and paralysis (Malone et al., 2016). ZIKV infection of pregnant women has severe conse-quences, including spontaneous abortions and newborns with microcephaly (Rasmussen et al., 2016). The social and economic burden of ZIKV is very severe. Given its burden on global health, antiviral treatments or effective vaccines for ZIKV are urgently needed. Some anti-ZIKV vaccines have shown promise (reviewed in Fernandez and Diamond, 2017), but establishing their safety and efficacy can take a significant amount of time and faces significant challenges (Rey et al., 2018). Small-mole-cule therapeutics against ZIKV should provide an important countermeasure alternative (Barrows et al., 2016; Xu et al., 2016), particularly if

they are also effective against related mos-quito-borne flaviviruses, such as dengue virus (DENV), which also causes devastating illness.

During infection, RNA viruses take over the host cell machinery to assist replication. Flavivirus such as ZIKV have a capped positive-sense single-stranded RNA genome of 11 kb that en-codes a single polyprotein. Co- and post-translational processing by the host and viral proteases generates three structural proteins (capsid, prM, and E) and seven nonstructural proteins (NS1, NS2A and 2B, NS3, NS4A and 4B, and NS5) (Apte-Sen-gupta et al., 2014; Lindenbach, 2007). The capsid protein encap-sidates the genomic RNA and is then enveloped by glycopro-teins prM and E to produce progeny virions (Kuhn et al., 2002; Pierson and Kielian, 2013). The nonstructural proteins participate in viral genome replication through the formation of multiprotein assemblies. All viral proteins are structurally complex and engaged in multiple functions and complexes (Hasan et al., 2018). With only ten proteins in its small RNA genome, ZIKV, like other RNA viruses, is entirely dependent on the host cell for replication and to generate the multiprotein complexes and virus-induced compartments involved in viral RNA synthesis and particle assembly (Nagy and Pogany, 2011).

Many antiviral strategies rely on directly targeting viral protein functions, including inhibitors of viral entry, viral polymerase, and viral proteases (De Clercq, 1996). Due to the very high mutational rate of most RNA viruses, drugs targeting viral proteins are often rendered ineffective due to the emergence of drug resistance (zur Wiesch et al., 2011). An alternative therapeutic concept for antivirals is to target host factors required by the virus (Lin and Gallay, 2013). The advantage of such approaches is that the drug target is not under the genetic control of the virus. Further, by targeting host functions required for replication of multiple virus families, such inhibitors may serve as broad-spectrum antivirals (Bekerman and Einav, 2015).

The host proteostasis machinery is universally required for the production of functional viral proteins (Maggioni and Braakman, 2005). Cellular protein homeostasis (or proteostasis) is normally maintained by a large array of molecular chaperones (Balch et al., 2008; Hartl et al., 2011; Kampinga and Craig, 2010).906 Cell Reports *26*, 906–920, January 22, 2019 [a] 2019 The Authors. This is an open access article under the CC BY-NC-ND license (http://creativecommons.org/licenses/by-nc-nd/4.0/). RNA viruses hijack this machinery to support viral replication, providing a target of pharmacological intervention. We have pre-viously shown that viral replication is hyper-dependent on the activity of certain chaperones (Geller et al., 2007, 2013; Taguwa et al., 2015). Viruses depend on few viral proteins using a subset of cellular chaperones, while host cells distribute the burden of folding a diverse range of proteins across a chaperone network. This feature of viral folding provides a therapeutic opportunity for the use of chaperone inhibitors to inhibit virus replication at doses that are relatively well tolerated in uninfected cells. Chaperones, including Hsp90 and Hsp70, are essential for replication of many clinically important viruses, including herpes simplex virus 1 and 2, influenza A, enteroviruses, respiratory syncytial virus, hepatitis B virus, Ebola virus, hepatitis C virus, and DENV (Chavez-Salinas et al., 2008; Geller et al., 2007, 2013; Hu and Seeger, 1996; Momose et al., 2002; Okamoto et al., 2006; Smith et al., 2010; Taguwa et al., 2015; Wright et al., 2009). Thus, available small-molecule inhibitors of

chaperones such as Hsp90 and Hsp70 could provide broad-spectrum antivirals (Neckers and Workman, 2012). An important advantage of this strategy is that viruses appear unable to develop drug resistance to antivirals targeting host chaperones (Geller et al., 2007, 2013; Taguwa et al., 2015).

Previously, we established that closely related flaviviruses, including DENV, yellow fever virus, West Nile virus, and tick-borne encephalitis virus, require the host Hsp70 chaperone ma-chinery to fold and assemble viral proteins (Taguwa et al., 2015). Hsp70 cooperates with defined sets of co-chaperones to mediate specific steps in the dengue viral life cycle, including entry, RNA replication, and capsid assembly (Taguwa et al., 2015; Yi et al., 2011). Importantly, drugs targeting host Hsp70 effec-tively block the replication of various flaviviruses with little toxicity to the host cell (Taguwa et al., 2015). These findings led us to examine whether targeting Hsp70 can provide a thera-peutic approach against ZIKV infection. We here show that Hsp70 plays a key role in ZIKV replication. Several cytoplasmic Hsp70 isoforms are recruited to viral-induced compartments and are required at distinct pre- and post-entry steps in the viral replication cycle. Accordingly, Hsp70 inhibitors effectively block viral replication in both human and mosquito cells without the emergence of drug resistance. Importantly, Hsp70 inhibitors protect mice from lethal ZIKV infection, demonstrating their potential for treatment and prevention of ZIKV disease.

RESULTS

Isoform-Specific Requirement of Cytosolic Hsp70s in ZIKV Replication

Cells contain multiple constitutively expressed and stress-inducible isoforms of cytoplasmic Hsp70s (herein generically termed Hsp70, unless noted). The specific roles of each isoform are not well understood. To assess the function of cytosolic Hsp70s in the ZIKV life cycle, we used a lentiviral system to establish five isoform-specific Hsp70 knockdown (KD) cells. These included HspA8, the constitutively expressed Hsp70 (also called Hsc70), ribosome-associated HSPA14, and three different stress-inducible isoforms (HSPA1, HSPA2, and HSPA6), which also express Hsp70 under unstressed conditions. Two previously characterized short hairpin RNAs (shRNAs) were used against each isoform; qRT-PCR of the relevant mRNAs established the efficiency of target gene KD (Figure S1A) (Taguwa et al., 2015). Following infection of these Hsp70 KD cells with the ZIKV MR766 strain, we examined viral RNA (vRNA) replication and infectious virus particle production 48 h post-infection (hpi). ZIKV infectious particle production was significantly suppressed by depletion of HSPA8 (Hsc70) (Figure 1A), the most abundant Hsp70 isoform in unstressed cells (Figure S1B). Smaller but significant decreases in extracellular infectious ZIKV particle production were observed upon KD of stress-inducible HSPA1 (also called Hsp70). In contrast, depletion of the stress-inducible HSPA2, or of the HSPA6 and HSPA14 iso-forms, did not significantly affect particle production (Figure 1A). Intracellular ZIKV vRNA levels (linked to RNA replication) were significantly reduced upon KD of HSPA1 and HSPA8, but not the other isoforms tested (Figure 1B). These results suggest that the two major cytoplasmic Hsp70 isoforms, HspA1 and HspA8, are required for the ZIKV life cycle.

Flavivirus infection generates viral-induced compartments that mediate various aspects of replication and assembly (Neu-feldt et al., 2018; Uchil and Satchidanandam, 2003). We find

that ZIKV infection remodels Hsp70 localization and recruits intracellular Hsp70s to virus-induced compartments. In unin-fected cells, cytoplasmic Hsc70 and Hsp70 (detected with anti-pan-Hsp-Hsc70 antibody) are diffuse throughout the cyto-plasm (Figure 1C). ZIKV infection recruits Hsc70 and Hsp70 to virus-induced structures containing the viral envelope protein E: the helicase NS3 and double-stranded RNA (dsRNA), which mark sites of vRNA replication (Figure 1C). To examine Hsp70 isoform-specific effects on ZIKV infection, we generated a panel of N-terminally GFP-tagged Hsp70 variants. Upon infection, GFP-HSPA8 (Hsc70) colocalized with puncta containing enve-lope protein E, suggesting a role in viral particle biogenesis (Figure 1D). The GFP-HSP1A (Hsp70) was also diffusely localized in uninfected cells but was recruited to NS3-containing structures (Figure 1E). Similar recruitment to E-containing structures was also observed for another constitutively expressed Hsc70, HSPA1L, which shares 90% identity with the inducible HSPA1 (Figure 1F). That different Hsp70 isoforms are recruited to distinct viral compartments presumably reflects their specific roles in the viral life cycle. Interestingly, GFP-HSP70 isoforms whose KD did not affect viral replication, such as HSPA1L (Figure 1F), HSPA2 (Figure S1C), HSPA6, and HSPA14 (not shown), were also recruited to ZIKV-induced structures. The lack of effect of their KD is likely due to the functional redundancy between various Hsp70 isoforms, where the more abundant HspA8 can partially replace their function. We conclude that a subset of Hsp70 isoforms is directly recruited to virally induced compartments and is required for ZIKV propagation.

Allosteric Inhibitors of Hsp70 Function Block Replication of Multiple ZIKV Strains

The folding action of Hsp70 is coupled to its ATPase activity, which is regulated by nucleotide exchange factors (NEFs; Figure S2A). We took advantage of allosteric inhibitors of the Hsp70-NEF interaction, including JG40, JG132, and JG345. These molecules from the same chemical series bind to a conserved allosteric site in all Hsp70s (Figures 2A) and impair the Hsp70 chaperone cycle by partially blocking NEF binding (Li et al., 2013, 2016). An advantage of these compounds over RNAi or KD approaches is that by targeting a conserved site, they can rapidly block the action of multiple Hsp70 isoforms. In these experiments, we used JG258 as a negative control, because it is structurally related to the other analogs but does not bind Hsp70. As a positive antiviral control, we used 2^0C-methyladenosine (2^0CMA; Figure 2A, NS5i), a nucleotide analog previously described as a Flavivirus-RNA-dependent RNA polymerase (RdRp) inhibitor (Olsen et al., 2004; Taguwa et al., 2015). The antiviral effect of these compounds was as-sessed in human Huh7 and mosquito C6/36 cells by measuring their effects on infectious particle production, as well as on viral protein and vRNA production. The Hsp70 inhibitors significantly suppressed production of infectious virus by three different ZIKV strains: the African MR766 strain, the Malaysian P6–740 strain, and the Puerto Rican PRVABC59 strain (Figures 2B and 2C). The compounds also blocked viral protein production (Figure S2B) and vRNA replication (Figures S2C and S2D). Of note, in human cells, ZIKV particle production was reduced more effectively by Hsp70 inhibitors than by the RdRp inhibitor 2^0CMA (Figures 2C and 2D). Importantly, the Hsp70 inhibitors showed relatively low toxicity (70%–100% survival) at the concentrations employed (Figure S2E), suggesting a good therapeutic window. Importantly, JG-258 was inactive in these assays, suggesting that the effect on ZIKV replication was due to Hsp70 inhibition (Figure S2F).

Testing multiple analogs indicates that despite targeting a highly conserved site in all Hsp70s, the best compound for one system may not always be the same for all cell and disease models. Indeed, we observed some differences between the action of these close analogs in human and mosquito cells. In human cells, JG40 effectively blocked viral protein and vRNA production for all ZIKV strains tested (Figures S2B and S2C), while JG345 had a more moderate effect on vRNA production (Figure S2C), despite being very effective at blocking virus production (Figure 2B). On the other hand, in mosquito cells, JG40 and JG132 significantly suppressed particle production of all strains tested but showed different levels of suppression of vRNA synthesis (Figures 2C and S2D). In mosquito cells, JG132 suppressed RNA replication in the MR766 and P6–740 strains, but not PRVABC59 strains, whereas JG40 showed little vRNA inhibition for all three strains (Figure S2D). Possible reasons for these differences likely include (1) differential association of different compounds with individual Hsp70 isoforms with distinct roles in each viral process/cell type, (2) differential expression of Hsp70 and/or NEFs in cell types, and (3) differential expression and/or binding of drug transporters. While beyond the scope of this particular study, a better understanding of these differences could potentially lead to more effective inhibition of viral replication. At present, we chose JG40 and JG345 for the further studies because of JG40's relatively broad spectrum and JG345's favorable pharmacokinetic properties (Moses et al., 2018; Shao et al., 2018).

Hsp70 Is Required at Multiple Steps in the ZIKV Life Cycle

To examine which steps of the viral life cycle require Hsp70, we performed time-of-drug addition experiments, which distinguish their roles in entry versus post-entry steps (Figure 3A). For reference, we compared JG40 to heparin (HP), a pan-flavivirus entry inhibitor, and 2^0CMA, an NS5 polymerase inhibitor that acts post-entry. These drugs were added before or after infection. As expected, HP suppressed ZIKV propagation, at the levels of vRNA and infectivity, when added during, but not after, viral entry, while 2^0CMA inhibited ZIKV replication only when added post-entry (Figure 3A). In contrast, JG40 significantly inhibited ZIKV propagation when added during or after entry, suggesting Hsp70 functions are required for both entry and post-entry steps of the ZIKV life cycle. By varying time-of-drug addition, experiments indicated Hsp70 may be required at distinct post-entry steps (Figures 3B–3D). JG40 was a more effective inhibitor of vRNA synthesis when added at the beginning of infection than when added at 2 hpi (86.8% reduction of vRNA synthesis compared to untreated when JG40 was added at t = 0 versus 64.2% reduction when JG40 was added 2 hpi). In contrast, we observed similarly strong inhibition of viral particle production whether JG40 was added pre- or post-infection (99.8% pretreatment versus 96.8% posttreatment reductions). We hypothesized these differences represent the distinct requirements of viral replication complex formation and viral particle assembly for Hsp70 activity. Replication complexes require Hsp70 action for their initial folding and assembly, but as infection progresses and the replication machineries are assembled, vRNA synthesis is less sensitive to JG40. In contrast, viral particle production or egress appears to be dependent on continued Hsp70 assistance.

To test the above hypotheses, we performed drug-chase experiments by adding JG40 at either 6 hpi (Figure 3B) or 24 hpi (Figures 3C–3F). First, Huh7 cells were infected with

ZIKV MR766 and either JG40 or 2^0CMA was added at 6 hpi, prior to any significant vRNA synthesis. The level of vRNA synthesis in the presence or absence of drugs was then monitored for up to 24 hpi. As expected, 2^0CMA fully abrogated vRNA synthesis compared to vehicle (Figure 3B). JG40 also inhibited vRNA synthesis, but to a smaller extent than 2^0CMA. This indicates that the establishment of an active viral replication state requires Hsp70 function.

Next, we added the drugs at 24 hpi and monitored the kinetics of ZIKV replication for an additional 12 h (Figure 3C). At this point, viral replication compartments in infected cells are already established. Nonetheless, 2^0CMA immediately suppressed new vRNA synthesis and slightly reduced capsid expression during the drug chase (Figures 3D and S3), as expected. In contrast, JG40 had no effect on ZIKV RNA or viral protein synthesis under these conditions. Together with the experiment in Figure 3B, these results indicate that Hsp70 is required to either fold or assemble the ZIKV replication complexes, but once the RNA replication machinery is assembled, ZIKV RNA synthesis no longer requires Hsp70 function. In contrast, the addition of JG40 at 24 hpi still significantly and immediately reduced the production of ZIKV infectious particles. Hsp70 inhibition caused a marked reduction in total virus load, as assessed upon cell lysis (Figure 3E) and in secreted viral titers in the supernatant from infected cells (Figure 3F). Strikingly, despite causing a dramatic block in vRNA synthesis, 2^0CMA-treated cells continued to produce and secrete infectious viral particles at untreated control levels. This suggests that during the initial 24 hpi, infected cells generate a large amount of vRNA that suffices to produce the bulk of viral progeny. Thus, a rapid production of vRNA appears to be followed by a slow particle biogenesis replication step, which requires additional time to complete virus progeny production. This characteristic renders virus replication less sensitive to the action of RdRp inhibitors soon after infection. At 24 hpi, JG40 has a negligible effect on vRNA production but still affects infectious particle assembly.

Functional Interaction of Hsp70 with ZIKV Capsid Protein

The role of Hsp70 in ZIKV particle production led us to examine the ZIKV-capsid-Hsp70 interaction. Flavivirus capsid is encoded by the N terminus of the polyprotein. A series of sequential cleavage events by the host signal peptidase and the viral NS2B and NS3 protease gives rise to two capsid forms: a precursor mem-brane-anchored form (herein ZIKV capsid 1–122 aa) and a processed cytosolic form (herein ZIKV capsid 1–104 aa), respectively (Figure 4A) (Byk and Gamarnik, 2016; Kuno and Chang, 2007). The capsid protein associates with lipid droplets (LDs) and is imported into the nucleolus (Byk and Gamarnik, 2016; Mori et al., 2005; Shang et al., 2018). The function of these capsid interactions is not fully defined, but evidence suggests that LD interactions contribute to particle assembly (Samsa et al., 2009) and nuclear import enhances host specific infectivity (Mori et al., 2005).

In initial experiments, we asked whether the capsid directly in-teracts with Hsp70. Both FLAG-tagged variants of the capsid were co-expressed with HSPA8 bearing a GFP cloned from copepod *Pontellina plumata* (herein cGFP) or control cGFP. FLAG immunoprecipitation followed by immunoblot detection indicated that both capsid forms specifically interact with HSPA8 (Figure 4A). Since inhibiting Hsp70 targets the capsid for

degradation in DENV (Taguwa et al., 2015), we examined ZIKV capsid stability in the presence or absence of Hsp70 inhibition. A significant reduction of both membrane-anchored and soluble capsid forms was observed upon JG40 treatment (Figure 4B). This reduction was abrogated by the inclusion of MG132, a proteasome inhibitor (Figure S4A).

Next, we examined the role of Hsp70 in the localization of ZIKV capsid LD and the nucleus (Figures 4C and S4B). In un-treated cells, FLAG-capsid was strongly colocalized with LD, as visualized by co-staining with the LD protein ADRP as well as the lipophilic dye BODIPY 493/503 (Figure 4C). Treatment with JG40 dramatically abrogated capsid association with LDs, indicating that Hsp70 activity is required for LD association. The localization of the capsid to nuclear puncta was only observed when cells were fixed with methanol, which also dissolves the LD (MeOH; Figure S4B). Addition of JG40 also reduced but did not eliminate the intensity of capsid puncta in the nucleus. These data suggest that Hsp70 activity is required for capsid protein stability and assembly into functional complexes.

To better understand the role of Hsp70 in capsid biology, ZIKV-infected cells were lysed in mild detergent (0.5% Triton-lX) and subjected to iodixanol gradient fractionation (Figures 4D and S4C), followed by immunoblot detection of capsid (Figures 4E–4G and S4D). In infected cells without drug treatment, the capsid migrated to two distinct positions in the gradient, with one pool toward the top of the gradient (Figures 4D and S4C; fraction 2) and another deeper in the gradient (fraction 8). The pool in fraction 2 also comigrated with the envelope protein, suggesting it may be a virion assembly precursor (Figure S4D). Fraction 2 also partially overlapped with the LD marker ADRP (Figure S4D).

The distinct capsid fractions identified in the iodixanol gradient also display different mobilities on blue-native PAGE, which separates native complexes by size (Figure 4F). The capsid in fraction 2 migrated as an 50-kDa species, while the capsid in fraction 8 was present in a series of high-molecular-mass species that barely migrated into the gel (Figure 4F). Treatment of in-fected cells with JG40 significantly reduced the capsid pool in fraction 2 (Figures 4E–G). The extent to which JG40 also affected the capsid species in fraction 8 was harder to ascertain given its heterogeneous nature and low mobility. Adding MG132 together with JG40 partially restored the accumulation of capsids in fraction 2 (Figures 4F, 4G, and S4A) but did not rescue the inhibitory effect of JG40 on viral titers (Figure 5A). No rescue was obtained by co-addition of MG132 and the lysosomal degradation inhibitor concanamycin A (CM); in fact, these degra- dation inhibitors mildly exacerbated the inhibitory effect of JG40 (Figure 5A) (Gilfoy et al., 2009). These experiments indicate that Hsp70 associates with ZIKV capsid, playing a key role in its native assembly and function.

Hsp70 Function Is Required to Produce Infectious Viral Particles

We next determined whether Hsp70 affects the infectivity of ZIKV viral particles that have been secreted from infected cells (Figures 5B and S5A–S5C). To distinguish the action on virion assembly from effects on viral genome replication or protein production, we infected human or mosquito cells for 24 or 36 h, respectively, to allow the cells to accumulate a significant pool of both vRNA and viral proteins. Under these conditions, infected cells can robustly support continuous virion secretion even after 2^0CMA addition (Figure S3). At this

time, cells were washed to remove preexisting virions, and JG40, JG345, JG132, or vehicle was added for an additional 12 h to monitor new virion production. The supernatants from these human and mosquito cells were then collected for quantification of the levels of vRNA, virion proteins, and infectious titer. From these measurements, we derived the ratio of viral infectivity to vRNA for virus produced in these cells following drug addition. Surprisingly, we found that treatment with either Hsp70 inhibitor (JG40 and JG345 or JG132) did not significantly reduce the levels of viral genome in the supernatant (Figure S5A), nor did they reduce the levels of virion proteins (Figure S5B). However, the Hsp70 inhibitors had a dramatic effect on virion infectivity in both human and mosquito cells (Figure S5C; note log scale), which resulted in several log reductions for the JG-compound treated cells when the infectivity/vRNA ratios were computed (Figure 5B). These results indicate that beyond being required for entry, viral replication, and capsid interactions, Hsp70 is also required to produce infectious viral particles. While defining the basis for lower infectivity will require structural studies of the Hsp70-treated virions, we carried out a series of analyses on the protein composition of virions in the supernatant of JG40-treated cells (Figures 5C and 5D). We found that Hsp70 does not affect the processing of prM to M (Figure 5C) and does not affect the levels of the proteins E and M in virions (Figure 5D). However, we did observe that JG40 treatment led to the appearance of a slower migrating capsid band at 24 kDa in addition to the 15kDa capsid band observed in untreated cells. Indeed, fractionation of supernatants on iodixanol gradients showed that in JG40-treated samples, virion infectivity, capsid, and E co-migrate together with this aberrant capsid band (Figures S5D and S5E). The alterations in the electrophoretic mobility of the capsid protein are suggestive of aberrant capsid morphogenesis upon Hsp70 inhibition.

Serial Passaging of ZIKV in Hsp70-Inhibitor-Treated Conditions Does Not Elicit Drug Resistance

The emergence of drug-resistant variants is a major obstacle for the development of effective antiviral therapies. We hypothe-sized that because Hsp70 participates in several different steps in the ZIKV cycle, ranging from entry to virion infectivity, it would be difficult for ZIKV to acquire enough mutations to develop resistance to Hsp70 inhibitors. To test this idea, we performed serial passage experiment in the presence of JG40 or 2^0CMA.The virus produced after 10 serial passages under these conditions was tested for its sensitivity to two drugs. We performed the passaging experiment three times independently using 2^0C-MA and JG40 (Figures 5E and S5F, experiments I–III). In each replica, the passaged ZIKV gradually evolved resistance to 2^0C-MA, allowing serial passaging at increased concentrations of 2^0CMA (e.g., 2 mM in passage 1 [P1] to 16 mM for P10; Figure 5Ei). In contrast, the three independent biological replicates of the JG40 passaging experiment never produced drug resistance against JG40, retaining full sensitivity to JG40 at P10 (Figure 5Eii).

Hsp70 Inhibitors Block ZIKV Replication in Disease-Relevant Human Cells

Chaperone levels may vary among cell types, with many cultured cells exhibiting elevated Hsp70 levels due to their transformed phenotype. It is thus important to test the antiviral efficacy of Hsp70 inhibitors in disease-relevant cells. ZIKV strains are transmitted from infected mother to fetus, where they replicate in neural stem cells causing congenital

malformations (Garcez et al., 2016; Rasmussen et al., 2016). Accordingly, a therapeutic application for these Hsp70 inhibitors could involve protection from ZIKV infection to trophoblast cells, which form the outer layer of a blastocyst and develop into a large part of the placenta, as well as to neural stem cells that will develop into neuronal lineages. The human trophoblast cell line JEG3 and human neural stem cells (hNSCs) derived from H9 (WA09) embryonic stem cells have been used as relevant models for ZIKV infection of trophoblast (Miner et al., 2016; Tabata et al., 2016) and fetal NSCs (Gladwyn-Ng et al., 2018), respectively. As JG40 and JG345 were toxic to these cells at higher concentrations (5 μM; Figure S6A), we restricted the treatment level to 1.65 μM, where toxicity was reduced (>80% survival). All three strains of ZIKV replicated robustly in both trophoblasts and hNSCs, and the Hsp70 inhibitors (JG40 and JG345) significantly inhibited vRNA and particle production in all three distinct ZIKV strains in both trophoblasts and hNSCs in a dose-dependent manner (Figures 6A, 6B, S6B, and S6C). In JEG3 trophoblast and neural cells, the Hsp70 inhibitor JG345 reduced Puerto Rico ZIKV titers by more than 6 orders of magnitude (Figures 6Aiii and 6Biii). These dramatic reductions were also observed at the vRNA level (Figures S6Biii and S6Ciii). Compared to the cultured cells above (Figure S2), we noticed that the Hsp70 inhibitors had a more dramatic effect on viral replication in these two clinically relevant human cell models. We hypothesize that this enhanced sensitivity might be due to their relatively lower levels of endogenous Hsp70 when compared to tumor-derived cells.

Hsp70 Inhibitors Protect Animal Models from ZIKV Infection

The potential of Hsp70 inhibitor for antiviral prophylaxis was next examined in a mouse model of ZIKV infection based on previous studies evaluating therapeutic efficacy against lethal ZIKV infection in immunocompromised mice (Sapparapu et al., 2016; Zmurko et al., 2016). The Puerto Rico strain was inoculated into IFNR-knockout (KO) mice (Ida-Hosonuma et al., 2005). We used 10^3 focus-forming units per mouse and clinical symptoms evaluated up to 14 days post-infection (dpi). JG345 was admin-istered daily at 3 mg/kg starting a day before the infection and compared to vehicle (Figure 6C). This dosing scheme was based on previously reported mouse pharmacokinetics and pharmaco- dynamics (Moses et al., 2018; Shao et al., 2018). Consistent with these previous studies, JG345 had minimal effect on body weight (<5% reduction) in treated animals (Figure S6D).

To avoid a bias in interpretation, we used an equal number of male and female mice in the experiments shown in Figures 6C–6E. However, we observed that female mice were more susceptible to ZIKV infection, similar to what has been reported using a different IRF3/7 double knockout (DKO) mouse model of ZIKV infection (Kawiecki et al., 2017). We thus also scored sepa- rately a female-only cohort, since their increased susceptibility leads to a more robust ZIKV phenotype that allowed us to better observe the protective effect of JG compounds (Figures S6E and S6F). All our analyses showed that JG345 treatment significantly protected against the mortality caused by ZIKV infection (Figure 6D). We also assessed the course of infection using a clinical score comprising a set of symptoms, including limb weakness and paralysis. Administration of JG345 decreased the clinical score in all cohorts examined (Figures 6E and S6E). We also evaluated the effect of JG345 administration on viral titers before the appearance of symptoms in mice. In three

independent experiments, JG345 treatment (3 mg/kg) significantly reduced blood viremia (Figures 6F and S6F), suggesting that protection from infection (Figures 6D and 6E) results from a direct inhibition of virus replication (Figure 6F). Taken together, these data are preclinical proof of concept indicating that Hsp70 inhibitors can be effective anti-ZIKV therapeutics with acceptable toxicity and low risk of drug resistance.

DISCUSSION

The recurring emergence of human pathogenic arbovirus epidemics, with no effective vaccines or therapeutics available, highlights the public need for ready-to-use broad-spectrum antivirals. Building on our previous finding that Hsp70 is broadly required for flavivirus replication (Taguwa et al., 2015), here we investigated the potential of Hsp70 inhibitors as anti-ZIKV thera-peutics. We find distinct host Hsp70 isoforms are recruited to virus-induced compartments. Hsp70 inhibitors effectively block viral replication without any appreciable toxicity to the host and without eliciting drug resistance. Hsp70 inhibitors protect mice from ZIKV-infection-related morbidity and disease, reducing viral load with tolerable toxicity. These experiments support the concept that Hsp70 inhibitors can provide an effective ther- apeutic and prophylactic strategy against flavivirus infections.

Developing antiviral antibodies or vaccine therapies and virus- targeted small molecules are lengthy and complex processes that require a deep understanding of virus mechanisms and biology. In the case of flaviviruses such as DENV and ZIKV, vaccine strategies can successfully control infection but can be problematic due to antibody-dependent enhancement of infection (Rey et al., 2018). Compounds targeting host functions widely used by all or most viral families, such as chaperones, could be attractive candidates for readily available treatments that do not require lengthy characterization of viral proteins. Our data indicate that flavivirus replication is extremely dependent on Hsp70 and thus very sensitive to Hsp70 inhibition, allowing complete block of viral propagation at concentrations with little toxicity to the host. We hypothesize this differential Hsp70 dependence arises from a number of characteristics of viral replication: (1) Viral proteins tend to be large and multifunctional (reviewed in Hasan et al., 2018) and thus are highly dependent on chaperone assistance for folding and assembly (Geller et al., 2012). (2) Viruses require chaperone assistance to remodel the host proteome and assemble elaborate cellular structures for vRNA and virion production (Maggioni and Braakman, 2005; Nagy and Pogany, 2011). (3) RNA viruses must produce large amounts of a small set of virus-encoded proteins, which places an unbalanced burden on a specific set of chaperones (Geller et al., 2012; Taguwa et al., 2015). In contrast, cellular folding distributes the substrate load across multiple chaperone families.(4) RNA viruses have extremely high mutation rates (Vignuzzi et al., 2006). This facilitates their adaptation and pathogenicity, but also generates many mutated variants dependent on proteostasis assistance. Since nonsynonymous mutations are mostly deleterious to protein stability (Balch et al., 2008; Hartl et al., 2011; Kampinga and Craig, 2010), even when beneficial in phenotype (Liu et al., 2017), this high mutational burden may enhance viral chaperone dependence.

We find that for ZIKV, similar to DENV virus, Hsp70 functions at distinct steps of the ZIKV life cycle: virus entry, formation of the active replication complex, and particle production.

Comparing the role of Hsp70 in the virus life cycle of ZIKV and other flavivirus reveals the subtle interplay between viral proteins and host pro- teostasis. Like ZIKV, DENV also requires Hsp70 to facilitate virus entry and particle production (Howe et al., 2016; Taguwa et al., 2015). However, DENV requires continued Hsp70 function for vRNA synthesis, while once the ZIKV replication complex is assembled, Hsp70 inhibitors no longer affect vRNA synthesis. In the case of Japanese encephalitis virus (JEV), Hsp70 is required for entry and replication complex formation (Ye et al., 2013). Given the high degree of similarity between these virus families, the distinct Hsp70 requirement of individual viral functions is intriguing and suggests that the degree of Hsp70 dependence may be regulated by slight variations in sequence or mechanism. However, entry and capsid maturation in flaviviruses appear to share a strict requirement for Hsp70 function. The role in entry has not been explored in detail but could in principle be linked to capsid uncoating (Byk et al., 2016; Goodwin et al., 2011). Hsp70 inhibition strongly affects capsid function, reducing its stability (Figure 4B), preventing its association with LDs (Figure 4C), and altering the formation of capsid complexes in the cell (Figure 4F). These effects, similar to what is observed for DENV capsid mutations disrupting helix formation (Teoh et al., 2014), indicate a role of Hsp70 in capsid folding or stability. The strong dependence of capsid biogenesis on Hsp70 likely stems from its strong hydrophobic core flanked by basic N- and C-terminal tails (Shang et al., 2018), typical motifs for Hsp70 binding (Kampinga and Craig, 2010). We find that even when administered late in infection, when viral protein and vRNA have already been produced, inhibitors of Hsp70 have a dramatic effect on virion infectivity, resulting in defective particles (Figure 5). Notably, we find that under these conditions, capsid in the virion has aberrant electrophoretic mobility, suggestive of an altered conformation. In addition to Hsp70, other chaperones, such as Hsp90 or TRiC, may also facilitate virus protein folding and assembly (Geller et al., 2012; Hafirassou et al., 2018; Inoue et al., 2011). The precise dependence of a given virus family for distinct classes of chaperones may depend on their topology and folding pathway.

For small-molecule antivirals, one of the most significant concerns is the rapid emergence of drug resistance (zur Wiesch et al., 2011). As observed for DENV, ZIKV sensitivity to Hsp70 inhibitors is maintained upon repeated passaging, without the emergence of drug resistance (Figure 3G), likely because its multifaceted involvement in the viral life cycle. Together with its broad action against multiple flavivirus families and moderate toxicity to the host, the low risk of drug resistance of these chaperone inhibitors makes them attractive antivirals for flavivirus treatment and perhaps for other viral infections. Our choice of prophylactic administration before the ZIKV challenge was guided by the limitations of current *in vivo* mouse model of ZIKV infection (Morrison and Dia- mond, 2017), which rely on immunocompromised mice with impaired interferon signaling (e.g., IFNAR KO and IRF3/5/7 triple knockout [TKO] [Lazear et al., 2016] or STAT2 KO [Tripathi et al., 2017]). This limitation makes the course of infection atypical when compared to human patients, where the immune system can cooperate with the antiviral treatment to clear the infection. Even in these immunocompromised mice, JG345 administration *in vivo* controls both Zika pathology and viremia. Our study provides a proof-of-concept preclinical example of a broad-spectrum anti-flaviviral drug that can open the way for the development of effective therapeutic interventions. Further tests in an animal model with a more robust im- mune

system (Gorman et al., 2018) may enhance the thera- peutic effect of these drugs if innate immunity acts in synergy with antiviral drugs for viral clearance.

STAR★METHODS

CONTACT FOR REAGENT AND RESOURCE SHARING

Further information and requests for resources and reagents should be directed to and will be fulfilled by the Lead Contact, jfrydman@stanford.edu.

EXPERIMENTAL MODEL AND SUBJECT DETAILS

Cells—Huh7 (hepatocellular carcinoma) and C6/36 (larva whole, Aedes albopictus) cells were cultured at 37 C and 32 C respectively as described in (Taguwa et al., 2015). JEG3 (Placenta Choriocarcinoma) cells were cultured as Huh7 cells. H9-derived human neural stem cells (hNSCs) were maintained in Knockout DMEM/F12 supplemented with 1mM GlutaMax-I and 2% StemPro hNSC SFM, 20ng/m bFGF and 20ng/ml EGF.

Viruses—ZIKV MR766, P6–740 and PRVABC59 strains stocks were produced and viral titers determined as described in (Taguwa et al., 2015). For passaging, 1×10^5 FFU MR766 viruses were serially propagated in the presence of 2^0CMA or JG40 in Huh7 cells at MOI = 0.5 for 4 days. At each passage the virus titers were measured and adjusted to 1×10^5 FFU for the next passage. Drug concentrations were gradually increased through the passages (2^0CMA; 3mM to 4, 8, and 16mM from passage 2, 3 and 5, JG40; 1mM to 1.5 and 2mM from passage 3 and 7, respectively). shRNA expressing lentivectors were generated as described previously (Taguwa et al., 2015).

Mice—Pathogen free Tg21 mice with type I interferon receptor knockout (Tg21/IFNR-KO) were bred and maintained in the AAALAC-certified animal facility at UCSF. Both male and female mice were used in all animal experiments conducted in accordance with the guidelines of Laboratory Animal Center of National Institute of Health. The Institutional Animal Care and Use Committee of the University of California San Francisco approved all animal protocols (Approved protocol No. AN156530–02).

METHOD DETAILS

Transfection, precipitation, PAGE and immunoblots—Cells were transfected using Fugene HD according to the manufacturer's protocol. Pull-down assays were performed according to the protocol previously described (Taguwa et al., 2015)

For immunoblotting, cells lysed in RIPA buffer (25 mM Tris-HCl, 150 mM NaCl, 1% NP-40, 0.5% Sodium deoxycholate, 0.1% SDS) were homogenized by ten passages through a 25-gauge needle. Protein concentration was determined by BCA assay and samples were adjusted with 1X SDS-sample buffer (50mM Tris-HCl pH7.4, 5% SDS and 10% Glycerol), and subjected to SDS-PAGE and western blot analysis using antibodies as indicated.

For Blue-Native PAGE, Samples were combined with 4X NativePAGE$^{\hat{a}}$ Sample buffer and NativePAGE$^{\hat{a}}$5%G-250 sample additive and run on a 4%–16% Bis-Tris gel (Invitrogen) at

100V for 180 min, transferred onto a PVDF membrane and capsid proteins were detected by western blot analysis using specific antibodies.

Quantitative Real-Time PCR (qRT-PCR)—Total cellular RNA was harvested using the RNeasy mini kit (QIAGEN). cDNA was synthesized using the High Capacity cDNA Reverse Transcription Kit (Life Technologies) qRT-PCR analysis was performed using gene-specific primers (Table S1) according to manu- facturers' protocols (iTaq™ Universal SYBR Green Supermix, Bio-Rad). Ct values were normalized to GAPDH mRNA in human cells, or 18S rRNA in mosquito cells.

Fluorescent microscopy—Cells cultured on glass slides were fixed in 4% paraformaldehyde-PBS or 100% ice cold Methanol for 15min and treated as described in (Taguwa et al., 2015). Slides were imaged using an LSM-700 scanning confocal microscope (Zeiss) and images were merged with ImageJ software.

Density gradient ultracentrifugation—Cells resuspended in TNE buffer (50mM Tris-HCl pH7.4, 150mM NaCl and 0.1 m EDTA) with protease inhibitor cocktail (Roche) were sheared by 25 strokes through 25G needle and mixed with equivalent 2% Triton-TNE buffer for 30min, at 4 C. Lysates were loaded on top of a 10% to 48% Iodixanol (OptiPrep; Sigma-Aldrich) gradient and subject to ultracentrifugation at 33,000 rpm in a SW40 swing- ing bucket rotor (Beckman Coulter) for 18 h at 4°C. 1ml fractions were collected by pipetting from top to bottom of the tube.

Experimental model: Animal experiments—Four-week-old Tg21/IFNR-KO mice were intraperitoneally (i.p.) inoculated with 1 3 10^3 pfu of ZIKV strain Puerto Rico. JG345 (1 or 3 mg per kg of mouse body weight), or 50 ml of solvent (10% DMSO, 18% Kolliphor RH 40, 3.6% dextrose in water) were daily injected from the day before viral infection. Body weight, health condition and survival were monitored daily. Health condition was scored as: 0, healthy; 1, ruffled fur and hunchbacked appearance; 2, wasting and limb weakness; 3, one-leg paralysis; 4, paralysis on both limbs, and presented as average clinical score.

QUANTIFICATION AND STATISTICAL ANALYSIS

Statistical significance was determined using two-tailed Student's t test analysis (Figures 1A, 1B, 3, 4B, 5B, 5E, S1A, 2F, 4A, 5B, 5E, and 5G) and one-way ANOVA with post hoc Tukey HSD test (Figures 2B, 2C, 5A, 6A, 6B, S2C, S2D, S6B, and S6C) for *in vitro* ex- periments. Log rank test and Mann-Whitney U-test were performed for *in vivo* survival rate (Figure 6D), and clinical scoring and viremia (Figures 6E, 6F, and S6F), respectively. p values were calculated by Microsoft Excel and the significance levels are as stated in the Figure legends.

Supplementary Material

Refer to Web version on PubMed Central for supplementary material.

ACKNOWLEDGMENTS

REFERENCES

Apte-Sengupta S, Sirohi D, and Kuhn RJ (2014). Coupling of replication and assembly in flaviviruses. Curr. Opin. Virol 9, 134–142. [PubMed: 25462445]

Balch WE, Morimoto RI, Dillin A, and Kelly JW (2008). Adapting proteo- stasis for disease intervention. Science 319, 916–919. [PubMed: 18276881]

Barrows NJ, Campos RK, Powell ST, Prasanth KR, Schott-Lerner G, Soto-Acosta R, Galarza-Muñoz G, McGrath EL, Urrabaz-Garza R, Gao J, et al. (2016). A screen of FDA-approved drugs for inhibitors of Zika virus infection. Cell Host Microbe 20, 259–270. [PubMed: 27476412]

Bekerman E, and Einav S (2015). Infectious disease. Combating emerging viral threats. Science 348, 282–283. [PubMed: 25883340]

Byk LA, and Gamarnik AV (2016). Properties and functions of the dengue virus capsid protein. Annu. Rev. Virol 3, 263–281. [PubMed: 27501261]

Byk LA, Iglesias NG, De Maio FA, Gebhard LG, Rossi M, and Gamarnik AV (2016). Dengue virus genome uncoating requires ubiquitina-tion. MBio 7, e00804–16. [PubMed: 27353759]

Chavez-Salinas S, Ceballos-Olvera I, Reyes-Del Valle J, Medina F, and Del Angel RM (2008). Heat shock effect upon dengue virus replication into U937 cells. Virus Res 138, 111–118. [PubMed: 18809444]

De Clercq E (1996). Chemotherapy of viral infections In Medical Microbiology, Fourth Edition, Baron S, ed. (University of Texas Medical Branch at Galveston).

Enfissi A, Codrington J, Roosblad J, Kazanji M, and Rousset D (2016). Zika virus genome from the Americas. Lancet 387, 227–228. [PubMed: 26775124]

Fernandez E, and Diamond MS (2017). Vaccination strategies against Zika virus. Curr. Opin. Virol 23, 59–67. [PubMed: 28432975]

Garcez PP, Loiola EC, Madeiro da Costa R, Higa LM, Trindade P, Delvecchio R, Nascimento JM, Brindeiro R, Tanuri A, and Rehen SK (2016). Zika virus impairs growth in human neurospheres and brain organoids. Science 352, 816–818. [PubMed: 27064148]

Geller R, Vignuzzi M, Andino R, and Frydman J (2007). Evolutionary con-straints on chaperone-mediated folding provide an antiviral approach refractory to development of drug resistance. Genes Dev 21, 195–205. [PubMed: 17234885]

Geller R, Taguwa S, and Frydman J (2012). Broad action of Hsp90 as a host chaperone required for viral replication. Biochim. Biophys. Acta 1823, 698–706. [PubMed: 22154817]

Geller R, Andino R, and Frydman J (2013). Hsp90 inhibitors exhibit resis-tance-free antiviral activity against respiratory syncytial virus. PLoS ONE 8, e56762. [PubMed: 23460813]

Gilfoy F, Fayzulin R, and Mason PW (2009). West Nile virus genome ampli- fication requires the functional activities of the proteasome. Virology 385, 74–84. [PubMed: 19101004]

Gladwyn-Ng I, Cordón-Barris L, Alfano C, Creppe C, Couderc T, Morelli G, Thelen N, America M, Bessières B, Encha-Razavi F, et al. (2018). Stress-induced unfolded protein response contributes to Zika virus-associ- ated microcephaly. Nat. Neurosci 21, 63–71. [PubMed: 29230053]

Goodwin EC, Lipovsky A, Inoue T, Magaldi TG, Edwards AP, Van Goor KE, Paton AW, Paton JC, Atwood WJ, Tsai B, and DiMaio D (2011). BiP and multiple DNAJ molecular chaperones in the endoplasmic retic- ulum are required for efficient simian virus 40 infection. MBio 2, e00101– e00111. [PubMed: 21673190]

Gorman MJ, Caine EA, Zaitsev K, Begley MC, Weger-Lucarelli J, Uc-cellini MB, Tripathi S, Morrison J, Yount BL, Dinnon KH 3rd., et al. (2018). An immunocompetent mouse model of Zika virus infection. Cell Host Microbe 23, 672–685.e676. [PubMed: 29746837]

Hafirassou ML, Meertens L, Umaña-Diaz C, Labeau A, Dejarnac O, Bonnet-Madin L, Kümmerer BM, Delaugerre C, Roingeard P, Vidalain PO, and Amara A (2018). A global interactome map of the Dengue virus NS1 identifies virus restriction and dependency host factors. Cell Rep 22, 1364. [PubMed: 29386121]

Hartl FU, Bracher A, and Hayer-Hartl M (2011). Molecular chaperones in protein folding and proteostasis. Nature 475, 324–332. [PubMed: 21776078]

Hasan SS, Sevvana M, Kuhn RJ, and Rossmann MG (2018). Structural biology of Zika virus and other flaviviruses. Nat. Struct. Mol. Biol 25, 13–20. [PubMed: 29323278]

Howe MK, Speer BL, Hughes PF, Loiselle DR, Vasudevan S, and Hay- stead TA (2016). An inducible heat shock protein 70 small molecule inhibitor demonstrates anti-dengue virus activity, validating Hsp70 as a host antiviral target. Antiviral Res 130, 81–92. [PubMed: 27058774]

Hu J, and Seeger C (1996). Hsp90 is required for the activity of a hepatitis B virus reverse transcriptase. Proc. Natl. Acad. Sci. USA 93, 1060–1064. [PubMed: 8577714]

Ida-Hosonuma M, Iwasaki T, Yoshikawa T, Nagata N, Sato Y, Sata T, Yoneyama M, Fujita T, Taya C, Yonekawa H, and Koike S (2005). The alpha/beta interferon response controls tissue tropism and pathogenicity of poliovirus. J. Virol 79, 4460–4469. [PubMed: 15767446]

Inoue Y, Aizaki H, Hara H, Matsuda M, Ando T, Shimoji T, Murakami K, Masaki T, Shoji I, Homma S, et al. (2011). Chaperonin TRiC/CCT partic- ipates in replication of hepatitis C virus genome via interaction with the viral NS5B protein. Virology 410, 38–47. [PubMed: 21093005]

Kampinga HH, and Craig EA (2010). The HSP70 chaperone machinery: J proteins as drivers of functional specificity. Nat. Rev. Mol. Cell Biol 11, 579–592. [PubMed: 20651708]

Kawiecki AB, Mayton EH, Dutuze MF, Goupil BA, Langohr IM, Del Piero F, and Christofferson RC (2017). Tissue tropisms, infection kinetics, histologic lesions, and antibody response of the MR766 strain of Zika virus in a murine model. Virol. J 14, 82. [PubMed: 28420392]

Kuhn RJ, Zhang W, Rossmann MG, Pletnev SV, Corver J, Lenches E, Jones CT, Mukhopadhyay S, Chipman PR, Strauss EG, et al. (2002). Structure of dengue virus: implications for flavivirus organization, maturation, and fusion. Cell 108, 717–725. [PubMed: 11893341]

Kuno G, and Chang GJ (2007). Full-length sequencing and genomic char- acterization of Bagaza, Kedougou, and Zika viruses. Arch. Virol 152, 687–696. [PubMed: 17195954]

Lazear HM, Govero J, Smith AM, Platt DJ, Fernandez E, Miner JJ, and Diamond MS (2016). A Mouse Model of Zika Virus Pathogenesis. Cell Host Microbe 19, 720–730. [PubMed: 27066744]

Li X, Srinivasan SR, Connarn J, Ahmad A, Young ZT, Kabza AM, Zui- derweg ER, Sun D, and Gestwicki JE (2013). Analogs of the allosteric heat shock protein 70 (Hsp70) inhibitor, MKT-077, as anti-cancer agents. ACS Med. Chem. Lett 4, 1042–1047.

Li X, Shao H, Taylor IR, and Gestwicki JE (2016). Targeting allosteric control mechanisms in heat shock protein 70 (Hsp70). Curr. Top. Med. Chem 16, 2729–2740. [PubMed: 27072701]

Lin K, and Gallay P (2013). Curing a viral infection by targeting the host: the example of cyclophilin inhibitors. Antiviral Res 99, 68–77. [PubMed: 23578729]

Lindenbach BDR (2007). Flaviviridae: the viruses and their replication Fields Virology, 5th Edition, Knipe DM and Howley PM, eds. (Lippincott-Raven), pp. 712–746.

Liu Y, Liu J, Du S, Shan C, Nie K, Zhang R, Li XF, Zhang R, Wang T, Qin CF, et al. (2017). Evolutionary enhancement of Zika virus infectivity in Aedes aegypti mosquitoes. Nature 545, 482–486. [PubMed: 28514450]

Maggioni C, and Braakman I (2005). Synthesis and quality control of viral membrane proteins. Curr. Top. Microbiol. Immunol 285, 175–198. [PubMed: 15609504]

Malone RW, Homan J, Callahan MV, Glasspool-Malone J, Damodaran L, Schneider Ade.B., Zimler R, Talton J, Cobb RR, Ruzic I, et al.; Zika Response Working Group (2016). Zika virus: medical countermeasure development challenges. PLoS Negl. Trop. Dis 10, e0004530. [PubMed: 26934531]

Miner JJ, Cao B, Govero J, Smith AM, Fernandez E, Cabrera OH, Garber C, Noll M, Klein RS, Noguchi KK, et al. (2016). Zika virus infection during pregnancy in mice causes placental damage and fetal demise. Cell 165, 1081–1091. [PubMed: 27180225]

Momose F, Naito T, Yano K, Sugimoto S, Morikawa Y, and Nagata K (2002). Identification of Hsp90 as a stimulatory host factor involved in influenza virus RNA synthesis. J. Biol. Chem 277, 45306–45314. [PubMed: 12226087]

Mori Y, Okabayashi T, Yamashita T, Zhao Z, Wakita T, Yasui K, Ha- sebe F, Tadano M, Konishi E, Moriishi K, and Matsuura Y (2005). Nuclear localization of Japanese encephalitis virus core protein enhances viral replication. J. Virol 79, 3448–3458. [PubMed: 15731239]

Morrison TE, and Diamond MS (2017). Animal models of Zika virus infection, pathogenesis, and immunity. J. Virol 91, e00009–17. [PubMed: 28148798]

Moses MA, Kim YS, Rivera-Marquez GM, Oshima N, Watson MJ, Beebe KE, Wells C, Lee S, Zuehlke AD, Shao H, et al. (2018). Targeting the Hsp40/Hsp70 chaperone axis as a novel strategy to treat castration-resis- tant prostate cancer. Cancer Res 78, 4022–4035. [PubMed: 29764864]

Nagy PD, and Pogany J (2011). The dependence of viral RNA replication on co-opted host factors. Nat. Rev. Microbiol 10, 137–149. [PubMed: 22183253]

Neckers L, and Workman P (2012). Hsp90 molecular chaperone inhibitors: are we there yet? Clin. Cancer Res 18, 64–76. [PubMed: 22215907]

Neufeldt CJ, Cortese M, Acosta EG, and Bartenschlager R (2018). Rewiring cellular networks by members of the Flaviviridae family. Nat. Rev. Microbiol 16, 125–142. [PubMed: 29430005]

Okamoto T, Nishimura Y, Ichimura T, Suzuki K, Miyamura T, Suzuki T, Moriishi K, and Matsuura Y (2006). Hepatitis C virus RNA replication is regu- lated by FKBP8 and Hsp90. EMBO J 25, 5015–5025. [PubMed: 17024179]

Olsen DB, Eldrup AB, Bartholomew L, Bhat B, Bosserman MR, Ceccacci A, Colwell LF, Fay JF, Flores OA, Getty KL, et al. (2004). A 7-deaza-adenosine analog is a potent and selective inhibitor of hepatitis C virus replication with excellent pharmacokinetic properties. Antimicrob. Agents Chemother 48, 3944–3953. [PubMed: 15388457]

Pierson TC, and Kielian M (2013). Flaviviruses: braking the entering. Curr. Opin. Virol 3, 3–12. [PubMed: 23352692]

Rasmussen SA, Jamieson DJ, Honein MA, and Petersen LR (2016). Zika virus and birth defects: reviewing the evidence for causality. N. Engl. J. Med 374, 1981–1987. [PubMed: 27074377]

Rey FA, Stiasny K, Vaney MC, Dellarole M, and Heinz FX (2018). The bright and the dark side of human antibody responses to flaviviruses: lessons for vaccine design. EMBO Rep 19, 206–224. [PubMed: 29282215]

Samsa MM, Mondotte JA, Iglesias NG, Assunçao-Miranda I, Barbosa-Lima G, Da Poian AT, Bozza PT, and Gamarnik AV (2009). Dengue virus capsid protein usurps lipid droplets for viral particle formation. PLoS Pathog 5, e1000632. [PubMed: 19851456]

Sapparapu G, Fernandez E, Kose N, Bin Cao, Fox JM, Bombardi RG, Zhao H, Nelson CA, Bryan AL, Barnes T, et al. (2016). Neutralizing human antibodies prevent Zika virus replication and fetal disease in mice. Nature 540, 443–447. [PubMed: 27819683]

Shang Z, Song H, Shi Y, Qi J, and Gao GF (2018). Crystal structure of the capsid protein from Zika virus. J. Mol. Biol 430, 948–962. [PubMed: 29454707]

Shao H, Li X, Moses MA, Gilbert LA, Kalyanaraman C, Young ZT, Chernova M, Journey SN, Weissman JS, Hann B, et al. (2018). Exploration of benzothiazole rhodacyanines as allosteric inhibitors of protein-protein interactions with heat shock protein 70 (Hsp70). J. Med. Chem 61, 6163–6177. [PubMed: 29953808]

Smith DR, McCarthy S, Chrovian A, Olinger G, Stossel A, Geisbert TW, Hensley LE, and Connor JH (2010). Inhibition of heat-shock protein 90 reduces Ebola virus replication. Antiviral Res 87, 187–194. [PubMed: 20452380]

Tabata T, Petitt M, Puerta-Guardo H, Michlmayr D, Wang C, Fang-Hoo- ver J, Harris E, and Pereira L (2016). Zika virus targets different primary hu- man placental cells, suggesting two routes for vertical transmission. Cell Host Microbe 20, 155–166. [PubMed: 27443522]

Taguwa S, Maringer K, Li X, Bernal-Rubio D, Rauch JN, Gestwicki JE, Andino R, Fernandez-Sesma A, and Frydman J (2015). Defining Hsp70 subnetworks in dengue virus replication reveals key vulnerability in flavivirus infection. Cell 163, 1108–1123. [PubMed: 26582131]

Teoh PG, Huang ZS, Pong WL, Chen PC, and Wu HN (2014). Main- tenance of dimer conformation by the dengue virus core protein a4-a4^0 helix pair is critical for nucleocapsid formation and virus production. J. Virol 88, 7998–8015. [PubMed: 24807709]

Tripathi S, Balasubramaniam VR, Brown JA, Mena I, Grant A, Bardina SV, Maringer K, Schwarz MC, Maestre AM, Sourisseau M, et al. (2017). A novel Zika virus mouse model reveals strain specific differences in virus pathogenesis and host inflammatory immune responses. PLoS Pathog 13, e1006258. [PubMed: 28278235]

Uchil PD, and Satchidanandam V (2003). Architecture of the flaviviral repli- cation complex. Protease, nuclease, and detergents reveal encasement within double-layered membrane compartments. J. Biol. Chem 278, 24388–24398. [PubMed: 12700232]

Vignuzzi M, Stone JK, Arnold JJ, Cameron CE, and Andino R (2006). Quasispecies diversity determines pathogenesis through cooperative interac- tions in a viral population. Nature 439, 344–348. [PubMed: 16327776]

Weaver SC, Costa F, Garcia-Blanco MA, Ko AI, Ribeiro GS, Saade G, Shi PY, and Vasilakis N (2016). Zika virus: History, emergence, biology, and prospects for control. Antiviral Res 130, 69–80. [PubMed: 26996139]

Wright CM, Seguin SP, Fewell SW, Zhang H, Ishwad C, Vats A, Lingwood CA, Wipf P, Fanning E, Pipas JM, and Brodsky JL (2009). Inhibition of simian virus 40 replication by targeting the molecular chaperone function and ATPase activity of T antigen. Virus Res 141, 71–80. [PubMed: 19200446]

Xu M, Lee EM, Wen Z, Cheng Y, Huang WK, Qian X, Tcw J, Kouznet- sova J, Ogden SC, Hammack C, et al. (2016). Identification of small-mole- cule inhibitors of Zika virus infection and induced neural cell death via a drug repurposing screen. Nat. Med 22, 1101–1107. [PubMed: 27571349]

Ye J, Chen Z, Zhang B, Miao H, Zohaib A, Xu Q, Chen H, and Cao S (2013). Heat shock protein 70 is associated with replicase complex of Japa- nese encephalitis virus and positively regulates viral genome replication. PLoS ONE 8, e75188. [PubMed: 24086464]

Yi Z, Sperzel L, Nürnberger C, Bredenbeek PJ, Lubick KJ, Best SM, Stoyanov CT, Law LM, Yuan Z, Rice CM, and MacDonald MR (2011). Identification and characterization of the host protein DNAJC14 as a broadly active flavivirus replication modulator. PLoS Pathog 7, e1001255. [PubMed: 21249176]

Zmurko J, Marques RE, Schols D, Verbeken E, Kaptein SJ, and Neyts J (2016). The viral polymerase inhibitor 7-deaza-2^0-C-methyladenosine is a potent inhibitor of in vitro Zika virus replication and delays disease progression in a robust mouse infection model. PLoS Negl. Trop. Dis 10, e0004695. [PubMed: 27163257]

zur Wiesch PA, Kouyos R, Engelstädter J, Regoes RR, and Bonhoeffer S (2011). Population biological principles of drug-resistance evolution in infec- tious diseases. Lancet Infect. Dis 11, 236–247. [PubMed: 21371657]

Highlights

- A distinct set of cytosolic Hsp70s are involved in ZIKV replication

- Hsp70 function is required at multiple steps of the ZIKV life cycle

- ZIKV entry and capsid assembly are hypersensitive to Hsp70 inhibition

- Hsp70 inhibitors protect clinically relevant human cells and animal models from ZIKV

Figure 1. Cytosolic Hsp70 Isoforms Are Involved in the ZIKV Life Cycle

(A and B) Depletion of cytosolic Hsp70 isoforms reduces Zika virus (ZIKV) replication. Indicated knockdown (KD) cells were infected with ZIKV MR766 at MOI 0.5; 48 h post-infection (hpi), supernatants were harvested and extracellular virus titrated by focus-forming assay (FFA) as described in STAR Methods (A). Intra- cellular RNA was harvested, and viral RNA and host GAPDH mRNA was measured by qRT-PCR (B). Data represent means ± SD of three independent exper- iments, each carried out in triplicate. *p < 0.01; **p < 0.005.
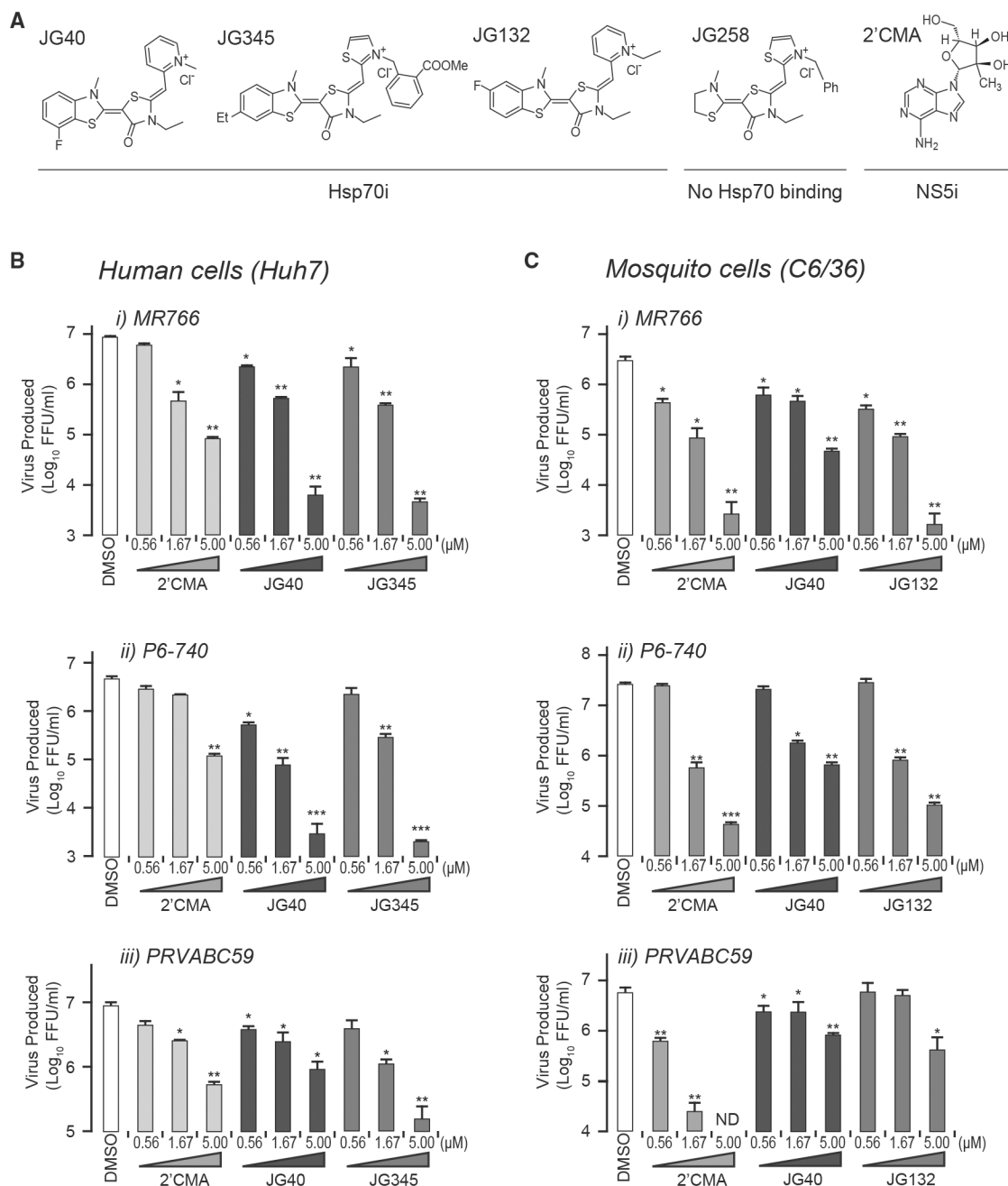
(C–F) Cytosolic Hsc70s and Hsp70s colocalize with ZIKV replication compartments. Huh7 cells infected with ZIKV MR766 were stained at 36 hpi with a pan- cytosolic HSC70 and HSP70 antibody (green); dsRNA, which marks viral replication sites (blue); and E or NS3 proteins (red) (C). Huh7 expressing GFP-HSPA8 (D), GFP-HSPA1 (E), or GFP-HSPA1L (F) cells were infected as in (C). Scale bars, 10 μm.

Figure 2. Hsp70 Functions Are Universally Required for ZIKV Propagation in Two Distinct Hosts: Human and Mosquito Cells

(A) Chemical structures of small compounds: JG40, JG345, and JG132, specific Hsp70 inhibitors; negative control, JG258; and 2^0CMA, a viral NS5 polymerase inhibitor.

(B and C) Hsp70 inhibitors suppress propagation of three ZIKV strains in human and mosquito cells in a dose-dependent manner. Huh7 (B) or C6/36 (C) cells were infected with (i) MR766, (ii) P6–740, and (iii) PRVABC59 at MOI 0.5 for 1 h, and inhibitors were added for 36 h (Huh7 cells) or 48 h (C6/36 cells). Extracellular virus infectivity was determined by FFA.
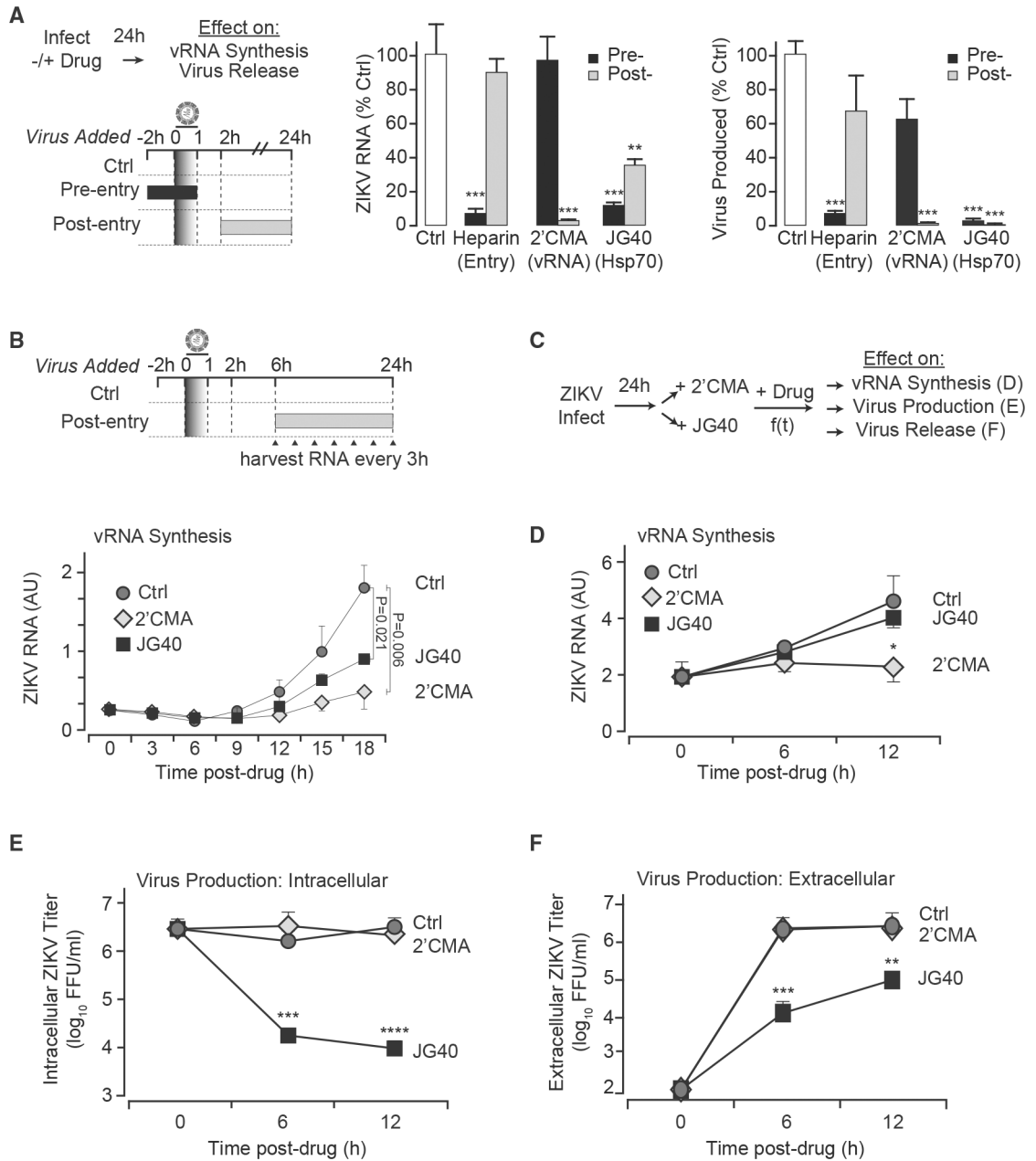
All data are expressed as means ± SD of three independent experiments, each carried out in triplicate, and analyzed by one-way ANOVA with post hoc Tukey honestly significant difference (HSD) test. *p < 0.05; **p < 0.01; ***p < 0.005.

Figure 3. Hsp70s Facilitate Two Distinct Steps in the ZIKV Life Cycle

(A) Hsp70 inhibition blocks viral entry and post-entry steps. Time-of-drug addition experiment with an Hsp70 inhibitor (JG40), entry inhibitor (heparin), and viral NS5 polymerase inhibitor (2^0CMA). Huh7 cells infected with ZIKV MR766 at MOI 0.5 were treated with inhibitors as indicated. Intracellular ZIKV RNA and extracellular virus infectivity was measured by qRT-PCR and FFA, respectively.

(B) Hsp70 is required for RNA replication during early infection. Huh7 cells were infected with ZIKV MR766 at MOI 0.5. At 6 hpi, cells were treated with 3 mM 2^0CMA or JG40, and intracellular viral RNA levels were monitored every 3 h.

(C–F) Hsp70 is required for infectious viral particle production of ZIKV. Drug-chase experiment comparing the effects of 2^0CMA and JG40 on viral RNA (vRNA) replication and virion production (C). Huh7 cells infected with ZIKV MR766 at MOI 0.5 were treated at 24 hpi with 3 mM 2^0CMA or JG40, and levels of intracellular ZIKV RNA

(D) and intra- and extracellular infectious virion levels

(E and F) were measured by qRT-PCR and FFA, respectively. All data are expressed as mean ± SD of three independent experiments. *p < 0.05; **p < 0.01; ***p < 0.005; ****p < 0.001.
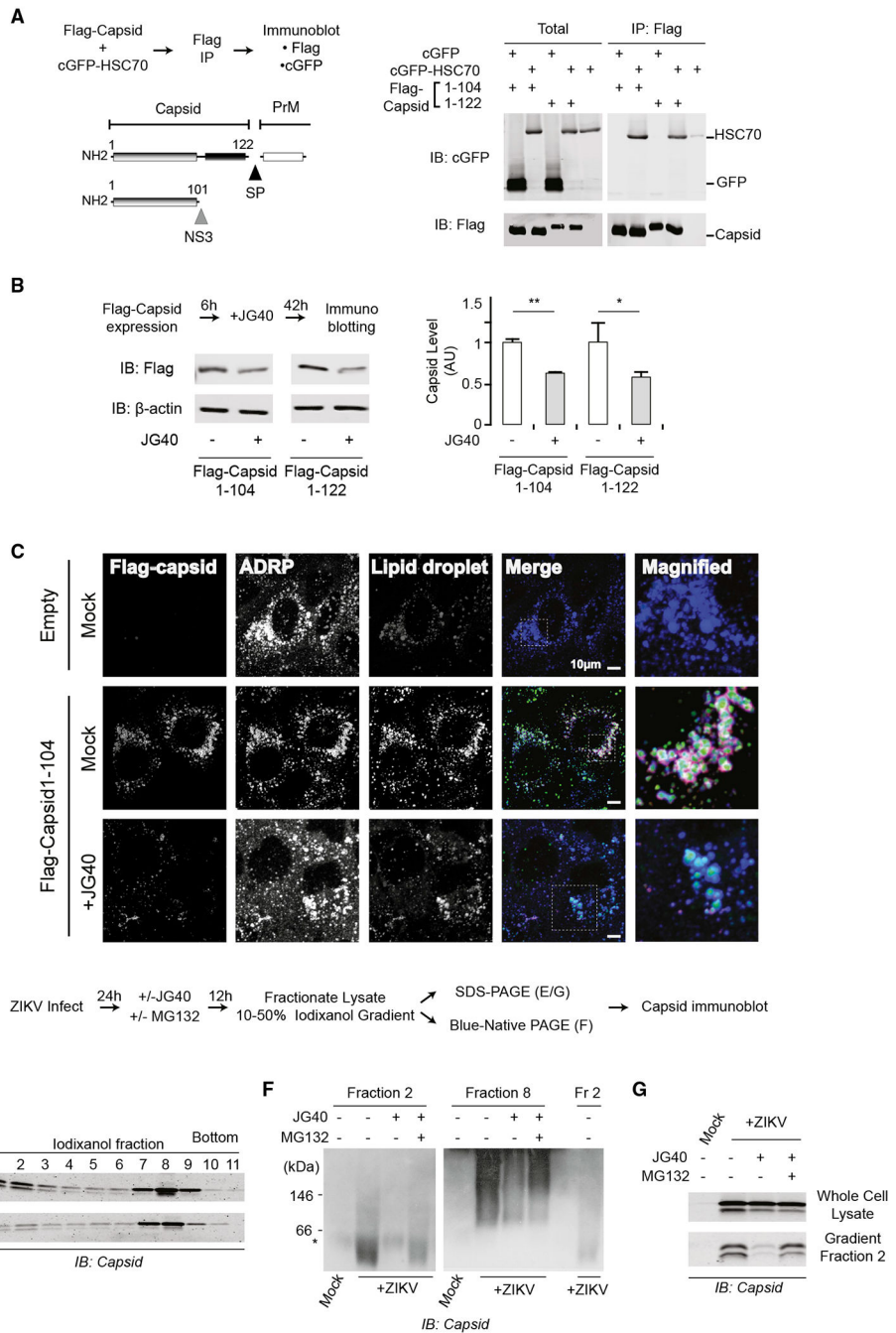
A

Flag-Capsid + cGFP-HSC70 → Flag IP → Immunoblot • Flag •cGFP

B

Flag-Capsid expression 6h → +JG40 42h → Immuno blotting

IB: Flag

IB: β-actin

JG40   -   +   -   +

Flag-Capsid 1-104   Flag-Capsid 1-122

C

Flag-capsid | ADRP | Lipid droplet | Merge | Magnified

Empty / Mock

Flag-Capsid1-104 / Mock

+JG40

10μm

D

ZIKV Infect 24h → +/-JG40 / +/- MG132 12h → Fractionate Lysate 10-50% Iodixanol Gradient ↗ SDS-PAGE (E/G) ↘ Blue-Native PAGE (F) → Capsid immunoblot

E

Top   Iodixanol fraction   Bottom
1 2 3 4 5 6 7 8 9 10 11

Mock

+JG40

IB: Capsid

F

Fraction 2   Fraction 8   Fr 2
JG40 -   -   +   +   -   -   +   +   -
MG132 -   -   -   +   -   -   -   +   -
(kDa)
146 -
66 -
*

Mock   +ZIKV   Mock   +ZIKV   +ZIKV

IB: Capsid

G

Mock   +ZIKV
JG40   -   -   +   +
MG132   -   -   -   +

Whole Cell Lysate

Gradient Fraction 2

IB: Capsid

Figure 4. Hsp70s Maintain Conformational Stabilization of Capsid and Its Localization on Lipid Droplets
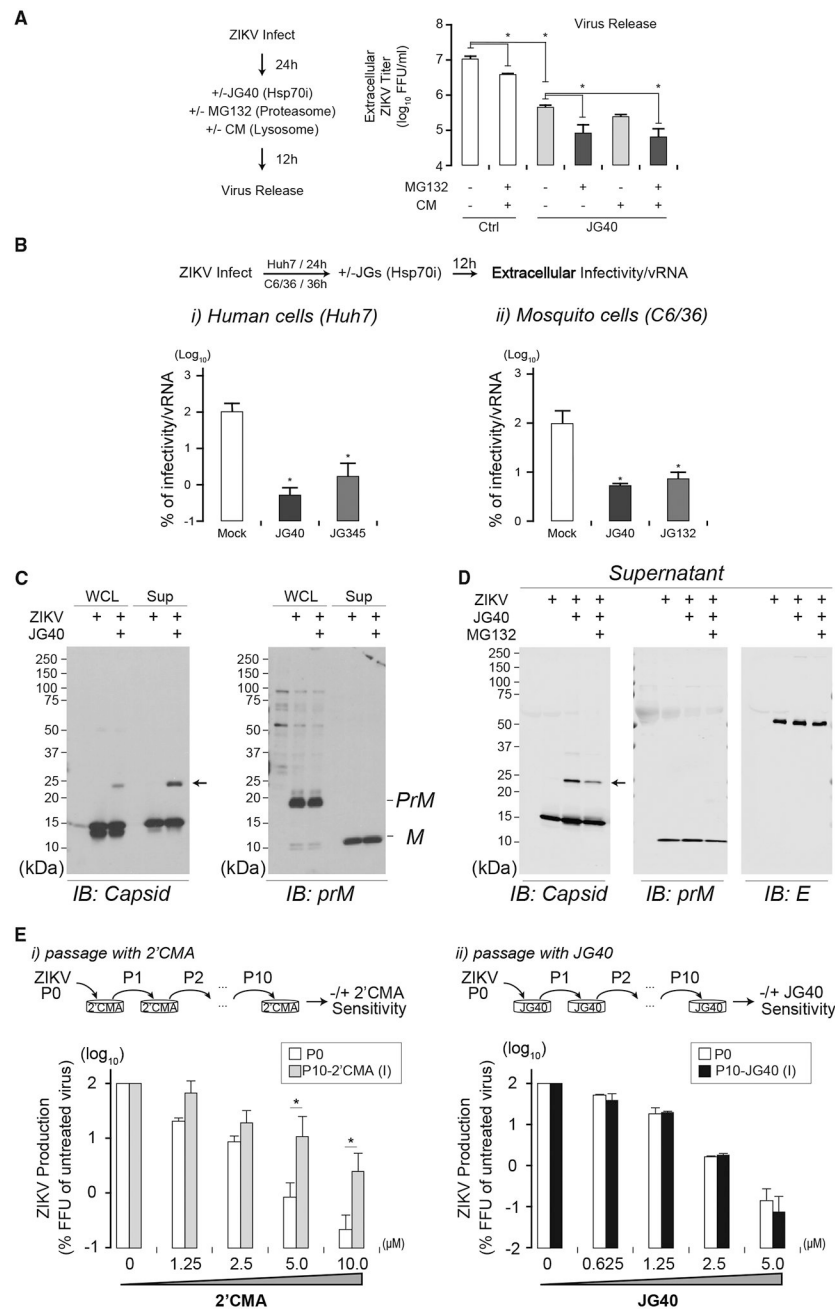
(A) Processed and unprocessed capsid variants physically associate with Hsc70. FLAG-tagged capsids were co-expressed together with GFP-tagged HSPA8 or control GFP in 293T cells, and their interactions were examined by co-immunoprecipitation.

(B) Hsp70 inhibition reduces expressions of processed and unprocessed capsids. FLAG-tagged processed and unprocessed capsid variants were expressed in Huh7 cells, and cells were treated with JG40 for 42 h. Cell lysates were subjected to immunoblot (left) and

quantified using infrared (IR) fluorescence on a Li-Cor Odyssey System (right). Data are mean ± SD of three independent experiments. *p < 0.05; **p < 0.01.

(C) Capsid localization to lipid droplets is decreased by Hsp70 inhibition. Huh7 cells stably expressing FLAG-tagged capsid 1–104 were treated with JG40 for 12 h, fixed by PFA, and permeabilized with saponin. FLAG-capsid (red) and ADRP (blue) were stained with specific primary antibodies, and the lipid droplets (green) were stained with BODIPY.

(D–G) Hsp70 inhibition reduces capsid levels in the light fraction of density gradients. (D) Scheme of experiments. At 24 hpi, Huh7 cells infected with ZIKV MR766 were treated with the indicated drugs for 12 h. Cell lysates were fractionated by iodixanol-gradient centrifugation. (E) Each fraction was subjected to SDS-PAGE followed by immunoblot. (F) Multimerization of the capsid is impaired under Hsp70 inhibition. Fractionated lysates as in (D) were subjected to blue-native PAGE and analyzed by immunoblot. (G) Effect of Hsp70 inhibition on capsid stability in the whole-cell lysate or fraction 2. Samples were subjected to SDS-PAGE and immunoblot as in (E).

A

B

i) Human cells (Huh7)

ii) Mosquito cells (C6/36)

C

IB: Capsid   IB: prM

D

IB: Capsid   IB: prM   IB: E

E

i) passage with 2'CMA

ii) passage with JG40

Figure 5. Involvement of Hsp70 Function in Infectious ZIKV Particle Production

(A) Blocking degradation does not abrogate JG40 inhibition of ZIKV propagation. Huh7 cells infected with ZIKV at MOI 0.5 were treated at 24 hpi with 3 mM CM and MG132 or JG40, and extracellular virion levels were measured by FFA.

(B) Hsp70 inhibition results in a reduced ratio of infectivity per particle. (i) At 24 hpi (Huh7) or (ii) 36 hpi (C6/36), ZIKV-infected cells were treated with the indicated Hsp70 inhibitors and incubated for 12 h. The ratio of infectivity to vRNA was calculated based on the amount of vRNA (Figure S5A) and infectivity (Figure S5B) in the supernatant.

(C) Post-translationally modified capsids incorporate into extracellular particles upon Hsp70 inhibition. ZIKV-infected Huh7 cells were treated with JG40 as in Figure 5B. The cells and supernatant were lysed and subjected to immunoblot analysis with anti-capsid (left) and anti-prM antibodies (right).

(D) Influence of Hsp70/proteasome inhibition on the incorporation of viral proteins into particles. ZIKV-infected Huh7 cells were treated with JG40/MG132 as in Figure 5B. The viral proteins in the supernatant were detected by immunoblot analysis.

(E) Serial passages of ZIKV MR766 in inhibitor-treated conditions to test the development of drug resistance. At each passage, Huh7 cells were infected with ZIKV at an MOI 0.5 in the presence or absence of JG40 or 2^0CMA. The sensitivity of inhibitors was examined for the indicated virus passages obtained as above using an MOI 0.5 to infect Huh7 cells. Extracellular infectivity was quantified by FFU assay. The passage experiments were performed three times independently (replica I is shown here, and replicas II and III are shown in Figure S5G).

All data are expressed as mean ± SD of three independent experiments. *p < 0.05.
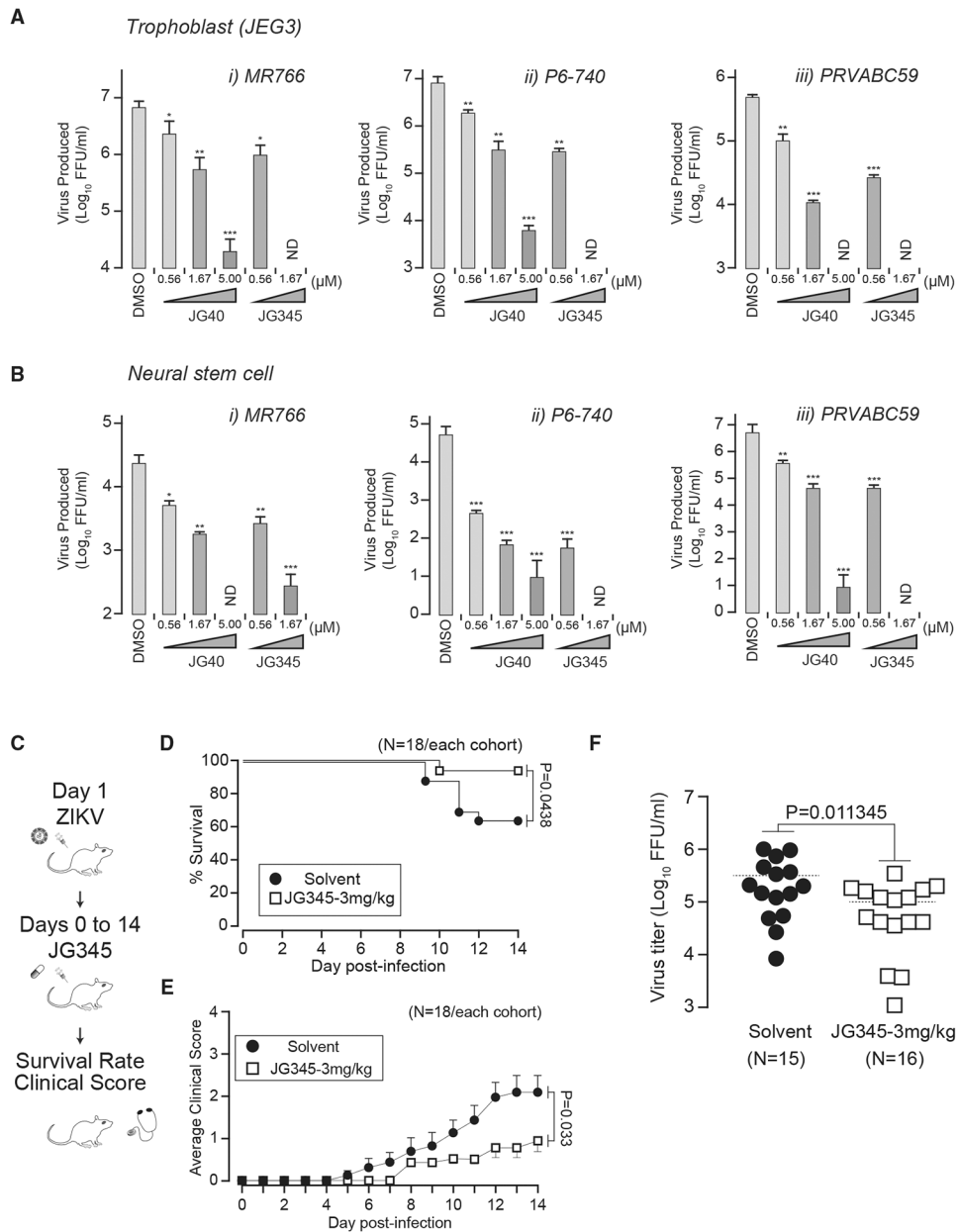
Figure 6. Hsp70 Inhibitors Suppress ZIKV Propagations in Clinically Relevant Cells and Protect Mice from Lethal ZIKV Infection

(A and B) Hsp70 inhibitors potently inhibit different ZIKV strains in clinically relevant cell lines. JEG3 cells (A) or H9-derived human neural stem cells (B) were infected with the ZIKV strains at MOI 0.5 and treated with JG compounds at the indicated concentrations for 48 h, and then infectivity was determined by FFA in Huh7 cells. Data are mean ± SD of three independent experiments. *p < 0.05; **p < 0.01; ***p < 0.005.

(C) Schedule of virus challenge in mice model.

(D) Survival rates of ZIKV-infected mice with solvent or JG345 at the indicated concentrations, monitored for 14 days. n = 18 in each cohort.

(E) Administration of Hsp70 inhibitor alleviates the clinical manifestation of ZIKV infection. Clinical score determination is described in STAR Methods. n = 18 in each cohort.
(F) At day 5, peripheral blood was harvested from ZIKV-infected mice, and infectivity in the serum was determined by FFA using Vero cells.

KEY RESOURCES TABLE

REAGENT or RESOURCE	SOURCE	IDENTIFIER
Antibodies		
Mouse Anti-HSP70/HSC70	Thermo Fisher scientific	Cat # MA3–014; RRID: AB_325462
Rabbit Anti-ZIKV CAPSID	GENETEX	Cat # GTX133317; RRID: AB_2756861
Rabbit Anti-ZIKV prM	GENETEX	Cat # GTX133584; RRID: AB_2756863
Rabbit Anti-ZIKV E	GENETEX	Cat # GTX133314; RRID: AB_2737413
Rabbit Anti-ZIKV NS3	GENETEX	Cat # GTX133309; RRID: AB_2756864
Rabbit Anti-ZIKV NS5	GENETEX	Cat # GTX133312; RRID: AB_2750559
Mouse Anti-dsRNA J2	SCICONS English & Scientific Consulting Kft.	RRID: AB_2651015
Mouse Anti-dsRNA K1	SCICONS English & Scientific Consulting Kft.	RRID: AB_2756865
Mouse Anti-St. Louis Encephalitis Antibody	Millipore	Cat # MAB8744; RRID: AB_11214431
Chicken Anti-ADFP	abcam	Cat # ab37516; RRID: AB_722641
Mouse Anti-ACTIN	Sigma-Aldrich	Cat # A5316; RRID: AB_476743
Rabbit Anti-TurboGFP	Thermo Fisher scientific	Cat # PA5–22688; RRID: AB_2540616
Mouse Anti-FLAG M2	Sigma-Aldrich	Cat # F3165; RRID: AB_259529
Goat anti-Mouse IgG, Alexa Fluor 405	Thermo Fisher scientific	Cat # A-31553; RRID: AB_221604
Goat anti-Mouse IgG, Alexa Fluor 488	Thermo Fisher scientific	Cat # A-11001; RRID: AB_2534069
Goat anti-Mouse IgM, Alexa Fluor 488	Thermo Fisher scientific	Cat # A-21042; RRID: AB_2535711
Goat anti-Rabbit IgG, Alexa Fluor 594	Thermo Fisher scientific	Cat # A-11037; RRID: AB_2534095
Goat anti-Chiken IgY, Alexa Fluor 594	Thermo Fisher scientific	Cat # A-11042; RRID: AB_142803
BODIPY 493/503	Thermo Fisher scientific	Cat # D3922
Bacterial and Virus Strains		
ZIKV strain:MR766	Gift from S Weaver & R Tesh	N/A
ZIKV strain:P6–740	Gift from S Weaver & R Tesh	N/A
ZIKV strain:PRVABC59	Gift from S Weaver & R Tesh	N/A
Chemicals, Peptides, and Recombinant Proteins		
JG40	Gift from Dr. J Gestwicki	N/A
JG132	Gift from Dr. J Gestwicki	N/A
JG345	Gift from Dr. J Gestwicki	N/A
JG258	Gift from Dr. J Gestwicki	N/A

REAGENT or RESOURCE	SOURCE	IDENTIFIER
Heparin	Sigma-Aldrich	Cat # H3393
2'C-methyladenosine	Carbosynth	Cat# NM0717
MG132	Calbiochem	Cat # 474790
Concanamycin A	Santa Cruz	Cat # sc-201111
VECTASTAIN Elite ABC anti-mouse IgG kit	Vector Laboratories	Cat # PK-6102
ImmPACT VIP peroxidase substrate	Vector Laboratories	Cat # SK-4605
Rneasy mini kit	QIAGEN	Cat# 74106
High Capacity cDNA Reverse Transcription Kit	Thermo Fisher scientific	Cat #4368813
iTaqTM Universal SYBR Green Supermix	Bio-Rad	Cat# 1725125
DMEM, high glucose, GlutaMAX Supplement	Thermo Fisher scientific	Cat # 10566016
MEM, GlutaMAX Supplement	Thermo Fisher scientific	Cat #41090036
KnockOut DMEM/F-12	Thermo Fisher scientific	Cat # 12660012
StemPro Neural Supplement	Thermo Fisher scientific	Cat# A1050801
Poly–L-ornithine hydrobromide	Sigma-Aldrich	Cat # P3655
Laminin	Sigma-Aldrich	Cat # L2020
Recombinant Human FGF-basic (154 a.a.)	PEPROTECH	Cat# 100–18B
Animal-Free Recombinant Human EGF	PEPROTECH	Cat# AF-100–15
Experimental Models: Cell Lines		
Huh7	Gift from Yoshi Matsuura	N/A
293T	ATCC	Cat # CRL-3216
C6/36	Gift from Yoshi Matsuura	N/A
JEG3	ATCC	Cat # HTB-36
StemPro Neural Stem Cells	Thermo Fisher scientific	Cat # A15654
Experimental Models: Organisms/Strains		
Mouse:B6 Tg21/IFNR-KO	Gift from Satoshi Koike	N/A
Oligonucleotides		
See Table S1 for the list of primers for qRT-PCR		N/A
Recombinant DNA		
See Table S2 for the list of Recombinant DNA		N/A
Software and Algorithms		
Image Studio Lite	Li-Cor	https://www.licor.com

REAGENT or RESOURCE	SOURCE	IDENTIFIER
ImageJ	NIH	https://imagej.nih.gov/ij/
Excel	Microsoft	N/A